ORIGINAL RESEARCH

Optimized antimicrobial and antiproliferative activities of titanate nanofibers containing silver

Yong Hua Su*
Zi Fei Yin*
Hai Liang Xin
Hui Qing Zhang
Jia Yu Sheng
Yan Long Yang
Juan Du
Chang Quan Ling

Department of Traditional Chinese Medicine, Changhai Hospital, The Second Military Medical University, Shanghai, People's Republic of China

*These authors contributed equally

Abstract: Titanate nanofibers containing silver have been demonstrated through the experiments reported herein to have effective antifungal and antiproliferative activities in the presence of UV light. The titanate nanofibers containing silver can be fabricated by means of ion exchange followed by a topochemical process in an environment suitable for reductive reactions. Excellent antibacterial, antifungal, and antiproliferative activities could be demonstrated by both $Ag_2Ti_5O_{11} \cdot xH_2O$ and Ag/titanate (UV light irradiation) due to their unique structures and compositions, which have photocatalytic activities to generate reactive oxygen species and capabilities to continuously release the silver ions. Therefore these materials have the potential to produce a membrane for the treatment of superficial malignant tumor, esophageal cancer, or cervical carcinoma. They may also hold utility if incorporated into a coating on stents in moderate and advanced stage esophageal carcinoma or for endoscopic retrograde biliary drainage. These approaches may significantly reduce infections, inhibit tumor growth, and importantly, improve quality of life and prolong survival time for patients with tumors.

Keywords: silver, titanate, photocatalytic, antiproliferative, antimicrobial

Introduction

Silver has long been known to be able to exhibit a strong toxicity to a wide spectrum of microorganisms with minimal perturbation to normal human cells. More specifically, silver ions have been revealed to be the most useful form of silver in terms of reported antibactericidal activity.[1–5] Before the introduction of the modern compounds containing silver, dilute solutions of silver nitrate were adopted to treat infections as early as in the nineteenth century. Nevertheless, silver existing in this form or in an ionic state in solution is not stable because the silver ions can easily be reduced to silver clusters, which results in significant loss of their antibactericidal effects. Silver-based compounds such as sulfadiazine silver ($C_{10}H_9AgN_4O_2S$) and mild silver protein (Argyrol®; Argyrol Pharmaceuticals, Seattle, WA) have been used extensively in various bactericidal applications.[6–9] For example, these silver-based compounds have been shown to be effective in the care of burns, severe chronic osteomyelitis, urinary tract infections, and central venous catheter infections.[10,11] Because these silver-based organic compounds are quite unstable, however, especially when exposed to heat or light irradiation, controlling dosage and obtaining consistent therapeutic outcomes is very challenging. Recently, other materials containing silver, such as Ag_2S/Ag heterodimers, silicon nanowires decorated with silver nanoparticles and Ag/SiO_2 nanocomposites, have been reported and some preliminarily antimicrobial

Correspondence: Chang Quan Ling
Department of Traditional Chinese Medicine, Changhai Hospital,
The Second Military Medical University,
168 Changhai Road, Shanghai, 200433
People's Republic of China
Tel +86 21 8187 1551
Fax +86 21 8187 1559
Email lingchangquan@smmu.edu.cn

1579

activities have been demonstrated.[12–14] One shortcoming of these systems relates to the relatively low concentration of silver ions present since they can be released only through the dissolution process. This is dependent on the surrounding environment and includes parameters such as pH, temperatures, solvents, redox conditions, and ionic strength. Indeed, even the storage time of composites containing silver could influence their release rate of silver ions.[4] Moreover, practical applications of various silver-based materials are often hampered by the ease of oxidation of silver nanoparticles to form silver oxide, which may cause loss of antibacterial activity.[5] Therefore, it is essential to design and construct a new carrier for stable silver ions which can store and release silver ions in a controllable manner.

Protonated titanate usually has a layered atomic structure which is clearly capable of exchanging ions, especially monovalent cations such as Na^+, K^+, Ag^+, and Cs^+.[15–18] The basic framework is built up from a structure unit of four TiO_6 octahedra arranged in a line by means of edge sharing. The units are combined with each other from above and below to form a zigzag string of octahedra. The formed string is then joined with other strings by corner sharing to make a staggered sheet containing 2-dimensional (2D) galleries inside.[19] Titanates of this structure have very pronounced ion-exchanging properties, allowing almost stoichiometric amounts of alkaline ions to be exchanged.[20–24] Due to its good biocompatibility, titanates have been used in various biological processes including biocatalysts, biosensors, controlled drug delivery, and bioscaffolds for cell cultures.[25–29] Furthermore, the light irradiation can cause titanates to generate reactive oxygen species (ROS) which are capable of damaging DNA, cell membranes, and cellular proteins,[5] and may lead to the death of microorganisms. The metallic silver nanoparticles growing on the surface of titanates can not only promote this photocatalytic process, but also enhance the absorption of the photons in the visible light region, to generate the ROS. The oxidation of silver nanoparticles can be avoided in the reductive chemical environment that was shaped during the photocatalytic process, thereby maintaining their antibacterial activity. By means of the above, the combination of the silver ions and the photocatalytic effects may serve to construct new functional materials for antimicrobial, antifungal, and antiproliferative applications, and potentially may also offer synergistic functions.

Herein, we report a facial synthesis process to prepare layered 1-dimensional (1D) titanates containing silver in different forms. The optimized forms of these materials were successfully screened for antimicrobial, antifungal, and antiproliferative applications. Through ion exchange and the controlled reduction processes, we demonstrate that silver species can be inserted into the layered titanates and then reduced to elemental silver nanoparticles. The average particle size and particle size distribution of silver nanoparticles can be tuned by using chemical ($NaBH_4$) or UV-light reduction processes. Interestingly, the experimental results indicate that silver titanate and Ag/titanate in the presence of UV-light irradiation have better antimicrobial, antifungal, and antiproliferative activities. These promising results indicate the synergistic effects that can be obtained through ROS being released from the photocatalysis process along with the silver ions that are released from the ion-exchange process. As a semiconducting material, layered titanates play a dual role, acting as a silver ion reservoir, as well as a photocatalyst.

Materials and Methods
Materials

All reagents used were of analytical grade. TiF_4 and the $NaBH_4$ were obtained from Sigma-Aldrich (St Louis, MO). All aqueous solutions were prepared with double-distilled water.

Synthesis of titanates and Ag/titanates

The layered protonated pentatitanate ($H_2Ti_5O_{11} \cdot H_2O$) was prepared according to a procedure reported previously.[30] In a typical experiment, 30 mL of 0.040 M TiF_4 aqueous solution containing 10 g of NaOH was kept in a Teflon-lined autoclave at 180°C for 48–50 hours and then the white gel-like product was washed thoroughly with a 0.50 M HCl solution and deionized water. To generate the Ag/titanate with the Ag^+ nutrients from the interlayer space, typically, 0.5 g of white $H_2Ti_5O_{11} \cdot H_2O$ product was added to 12.5 mL of $AgNO_3$ aqueous solution with a concentration of 0.01–0.1 M and stirred vigorously in the dark for 30–52 hours. In the wake of the H^+/Ag^+ exchange, the sample was washed thoroughly with deionized water to remove externally adsorbed Ag^+. Afterwards, the titanate with Ag^+ in the galleries was redispersed in 25 mL of deionized water and exposed to UV light (Xe 300 W, 320–400 nm) for 8–14 hours. As a parallel reduction method, $NaBH_4$ aqueous solution (0.02–0.05 M) was applied and stirred vigorously for 20 minutes. After the reaction, the Ag/titanate nanocomposites were washed with deionized water three times. It should be noted that all the ion-exchange and redox processes were performed at room temperature.

Characterization methods and instruments

Scanning electron microscopy with energy-dispersive X-ray spectroscopy (SEM/EDX, JSM-5600 LV [JEOL, Tokyo, Japan]; FESEM/EDX, JSM-6700F [JEOL]) and transmission electron microscopy (TEM, JEM 2010, 200 kV [JEOL]) were used to examine the dimension, morphology, and chemical composition of the samples. Surface binding elements were analyzed with X-ray photoelectron spectroscopy (XPS, Kratos Axis Ultra DLD, Manchester, UK). All binding energies were referenced to the C1s speak (285.0 eV) arising from surface hydrocarbons (or possible adventitious hydrocarbon). Prior to peak deconvolution, X-ray satellites and inelastic background (Shirley-type) were subtracted for all spectra. The UV-vis absorption spectra of protonated pentatitanate, silver titanate, and Ag/titanate nanostructures were examined with a UV-vis spectrophotometer (Cary-500; Varian Inc, Palo Alto, CA).

Antibacterial activity assay

E. coli DH-5α was selected as an indicator experimental bacteria. Luria Bertani (LB) broth was used as the culture medium. Bacteria were aerobically cultivated in LB broth for 20 hours at 37°C. A sterile cotton swab was used to inoculate E. coli DH-5α on to the surface of LB broth plates. The titanate-based compounds (2 mg) were suspended in sterile water and placed over the surface of the plates to keep in contact with E. coli. Each compound was divided into two groups, with one group being kept in the dark while the other was exposed to natural light for 2 hours per day. We took this approach so that the bacteria would not be killed by ultraviolet rays and the compounds could be excited by the minimal ultraviolet light present in the natural light. The diameter of inhibition zone was measured after 24 hours of incubation at 37°C, which enabled evaluation of the antibacterial activity.

Antifungal activity assay

To assess antifungal activity, the in vitro minimal inhibitory concentrations (MICs) of the titanate-based compounds were determined by using Candida albicans strain SC5314. These yeast cells were cultivated on Yeast Extract Peptone Dextrose (YPD) medium plates at 30°C overnight to obtain single colonies. These single colonies were then resuspended in YPD broth to a density of 1.0×10^8 cells/mL. The MICs of the cells were determined by a microdilution test based on the macrodilution referential method of the National Committee for Clinical Laboratory Standards.[31] Cells (100 μL; 5.0×10^4 cells/mL)

were then added into wells in a 96-well plate in rows A and B. Row A contained 200 μL of yeast cells and the titanate-based compounds for testing, while row B contained 200 μL of yeast cells only. Row C contained 200 μL of RPMI 1640 medium (Gibco, Langley, OK) as a blank control while row D contained 200 μL of RPMI 1640 medium, as well as titanate-based compounds. The titanate-based compounds to be tested were dispersed in phosphate buffer solution (PBS) and the two-fold serial dilutions were prepared in RPMI 1640 medium with a final concentration ranging from 200 to 0.390 μg/mL. Fluconazole (FLC) served as the positive control with final concentrations ranging between 64.0 and 0.125 μg/mL. Each titanate-based compound was divided into two groups with one group being kept in the dark while the other was exposed to ultraviolet light (λ = 365 nm, UVA, ENF-280C/FE, Spectroline, Westbury, NY) for 2 hours. The plates were then incubated at 30°C for 24 hours without being shaken and the growth of cells was determined by measuring the optical density at wavelength of 620 nm. The MIC$_{80}$ and MIC$_{50}$ of the target additives (titanate-based compounds or FLC) were defined as an approximately 80% and 50% reduction in terms of the growth of cells compared with the growth of cells with no target additive.

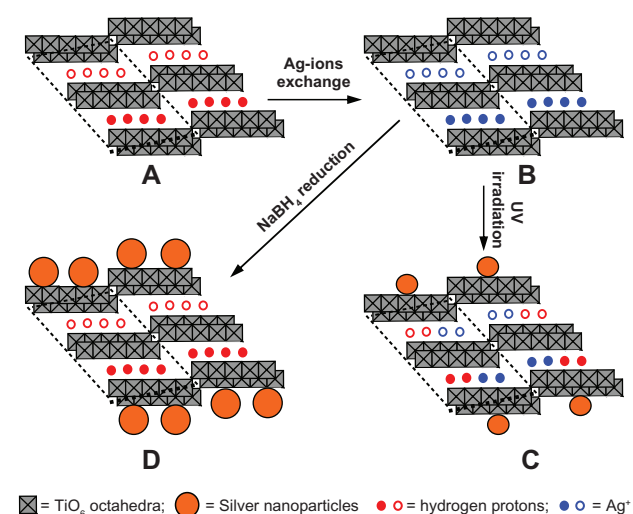## Antiproliferative activity assay

The in vitro antiproliferative activities of protonated pentatitanate ($H_2Ti_5O_{11} \cdot H_2O$) and corresponding silver-containing titanate nanofibers were studied on a human liver cancer cell line (Hep G2) by employing the Alamar Blue assay.[32,33] Parallel control groups without titanate-based inorganic compounds were also studied. Each titanate-based compound was further separated into two groups, with one group being kept in the dark while the other was exposed to ultraviolet light (λ = 365 nm, UVA) for 2 hours per day. Hep G2 cells were cultivated in DMEM and 10% fetal bovine serum (FBS) at 37°C in 5% CO$_2$. Cells were then added into 96 well plates (1×10^5 cells/mL, 100 μL) and the medium was replaced with DMEM and 10% FBS containing titanate-based compounds 24 hours later. Titanate-based compounds were tested over concentrations ranging from 3.125 μg/mL to 200 μg/mL. Then cells were incubated for 24 hours before 10 μL Alamar Blue was added and the plates were then incubated in the dark for a further 4 hours. Mitomycin C (MMC) was used as positive control in the cell viability assays. The optical density was monitored at 570 nm (absorbance) and 630 nm (reference absorbance) in a microplate reader (Elx-808; Biotek, Winooski, VT). The calculated IC$_{50}$ values were expressed as the concentration of titanate-based compounds

(μg/mL) under which 50% of cell death was observed, compared with the controls.

Results and discussion

A series of experiments was conducted to prepare silver titanate and Ag/titanate nanocomposites with the process shown in Scheme 1. The major steps involved are: (a) initial protonated pentatitanate with ion-exchanging capabilities (idealized structure viewed in the [010] direction; open and filled red circles denote H^+ or H_3O^+ at y = 0 and 1/2, respectively); (b) replacement of proton H^+ by Ag^+ in the interlayer space (open and filled blue circles denote Ag^+); and (c) partial intercalated Ag^+ cations were transferred to the outside of the galleries and then reduced to form silver clusters/nanoparticles by using titanates as the heterogeneous nucleation substrate. Some water molecules may also exist in the galleries in a quasi-liquid state, but these are not shown in the diagram. It should be noted that another similar process, reduction with $NaBH_4$, can be applied to the same cations to form more, relatively large, silver nanoparticles growing on the layered substrate. The basic structure of host lamellar $[Ti_5O_{11}{}^{2-}]_\infty$ does not change throughout the process from (A) to (C) in Scheme 1, except that the interlayer distance may vary with the degree of cation interaction, as well as by the amount of free interlayer water introduced.

Figure 1 shows the TEM images (A–D) and corresponding digital camera photographs (e–h) of the: initial protonated

Figure I TEM images and digital camera photographs of protonated pentatitanate ($H_2Ti_5O_{11}\cdot H_2O$) (**A** and **E**), titanate after Ag^+ cations exchange (**B** and **F**), partial reduction of Ag^+ cations from the layered space with the UV light irradiation (**C** and **G**), and reduction of Ag^+ cations with $NaBH_4$ agent (**D** and **H**).

pentatitanate ($H_2Ti_5O_{11}\cdot H_2O$) nanofibers as the starting structural basis (A); fully Ag^+ exchanged titanate (B); controlled partial reverse Ag^+ exchange and generation of Ag nanoparticles on titanate substrate through interlayer mass transfer and outside redox process in UV-light irradiation (C); and the product of fully reverse Ag^+ exchange and silver nanoparticles growth (D). The detailed information on preparation, structure, and properties of pristine protonated titanate ($H_2Ti_5O_{11}\cdot H_2O$) was illustrated in a previous publication; the bulk product dispersed in water appears as a stable milky solution, as indicated in the digital camera image (E).[30] Due to its layered structure and high ion-exchanging capability, the protonated titanate nanofibers can be used as an excellent Ag^+ nutrients reservoir, as well as a template for further silver nanoparticles growth.

Titanate with fully Ag^+/H^+ exchange was easily prepared by dispersing $H_2Ti_5O_{11}\cdot H_2O$ nanostructures in $AgNO_3$ aqueous solution (0.01–0.1 M) and stirring this vigorously in the dark for 30 hours at room temperature. The silver titanate generated maintains the original nanofiber morphology well, with a relatively clean surface, meaning that no silver nanoparticles are present at this stage (see Figure 1B). Compared with the original pure protonated titanate, the corresponding photograph of silver titanate (see Figure 1F) shows a very slight yellowness. The XPS data also support the conclusion that all of the silver is in the monovalent state (see Figure 3A). Interestingly, if

☒ = TiO_6 octahedra; ⬤ = Silver nanoparticles ● ○ = hydrogen protons; ● ○ = Ag^+

Scheme I Schematic representations of "nutrients from galleries" principle to generate Ag/titanate nanocomposites: (**A**) represents the pristine protonated pentatitanate ($H_2Ti_5O_{11}\cdot H_2O$); (**B**) silver titanate ($Ag_2Ti_5O_{11}\cdot xH_2O$) prepared by exchange of protons with Ag^+ cations; partial (**C**) or fully (**D**) Ag^+ cations exchange with protons in the layered space and the formation of the silver nanoparticles on titanate substrates with the redox process. The unit cell (a–d; enclosed by dotted lines) are C-based centered monoclinic, which is projected along [010] direction.
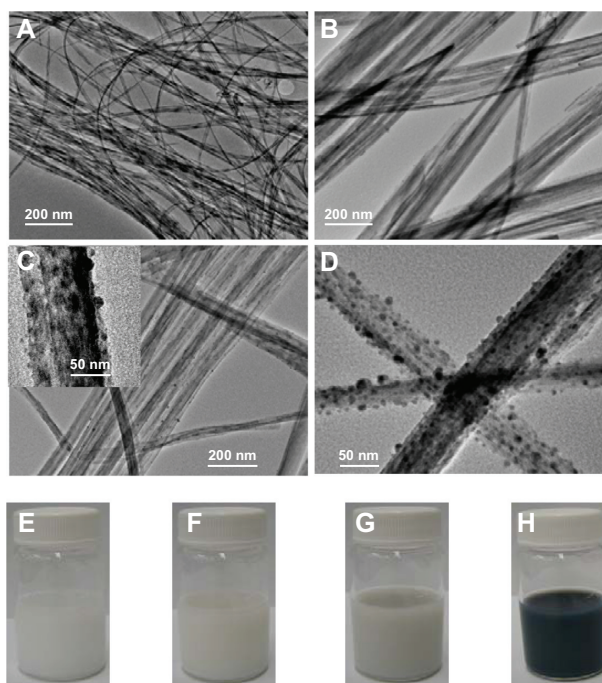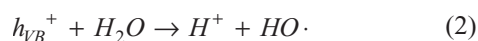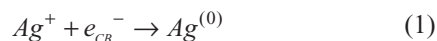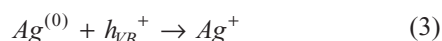**Note:** Open and filled circles indicate the locations at y = 0 and ½, respectively.

UV-light irradiation (300 W Xe, 320–400 nm) was applied to the as-prepared silver titanate aqueous solution, the color of the silver titanate would gradually change from slightly yellow to grey within 8–14 hours, as illustrated in Figure 1G. Based on the TEM observation in Figure 1C, the change of color is mainly caused by the formation of silver nanoparticles on titanate substrate, so that we can conclude that Ag^+ cations should be transferred from the galleries and then reduced by UV light. In UV-light irradiation, the photocatalytic nature of layered titanate can release reducing species, according to:

$$Ag^+ + e_{CB}^- \rightarrow Ag^{(0)} \quad (1)$$

$$h_{VB}^+ + H_2O \rightarrow H^+ + HO\cdot \quad (2)$$

even though

$$Ag^{(0)} + h_{VB}^+ \rightarrow Ag^+ \quad (3)$$

process may also exist in the presence of oxygen. As is revealed by the TEM image in Figure 1C, silver nanoparticles randomly grow on the titanate nanofibers and are approximately 10–20 nm with a spherical or hemispherical morphology. The high-resolution TEM (HRTEM) image shown in Figure 2 also provides evidence of the metal silver nanoparticles deposited on the titanate substrate. Measuring the lattice fringes of the HRTEM image shows that these were spaced at 0.25 nm on average, which is very close to the {111} lattice spacing of the face-centered cubic (fcc) silver crystals. Furthermore, the lattice spacing
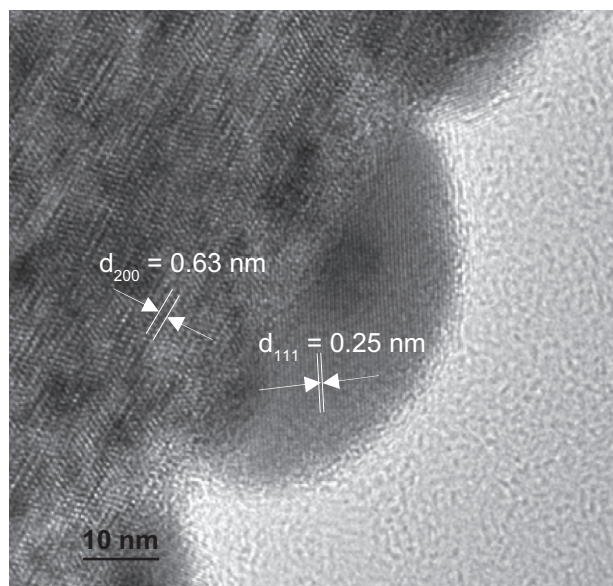
of the 1D titanate substrate is 0.63 nm on average (see Figure 2). Due to the meso-stable crystal structure, as well as surface properties of the titanate, zero valence silver clusters could easily form the nuclei on titanate nanofibers. Based on the TEM results (see Figure 1c), the silver ions did not penetrate too deeply into the bulk solution before they were reduced to a zero valance state, at which point they formed nanoparticles on the surface of the titanate substrate. Considering the ion balance inside the galleries, the H^+ or H_3O^+ produced by the redox reaction could be exchanged into the galleries in the process of the reaction, resulting in distortion of titanate lattice (see Figure 2). Therefore, in the current step, the cation exchange and the redox reaction are dynamic processes. Each stage of the process could be executed in a controllable way by adjusting external parameters such as UV-light intensity or irradiation time.
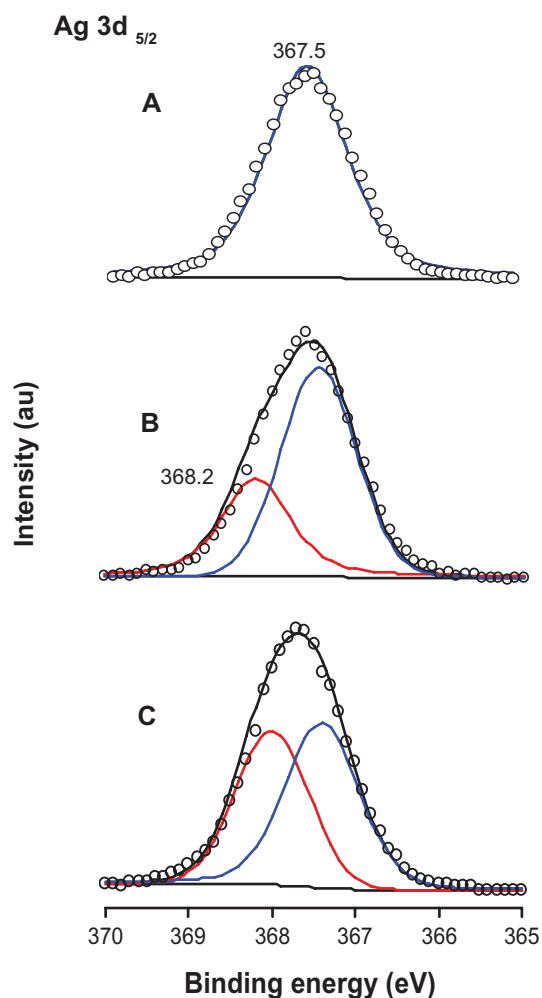

Figure 2 High resolution TEM image of Ag/titanate nanocomposite formed by UV light irradiation (300 W Xe, 320–400 nm).

Figure 3 X-ray photoelectron spectroscopy spectra of Ag 3d: (**A**) titanate after Ag^+ cation exchange, (**B**) partial reduction of Ag^+ cations from the layered space with UV light irradiation, and (**C**) reduction of Ag^+ cations with $NaBH_4$ agent.
Abbreviation: au, arbitrary units.

The XPS analysis indicates that about 34.84% of the silver cations have been reduced to a zero valence state, as shown in Figure 3b. Moreover, the release of Ag^+ nutrients from the galleries and the following redox process could be more thoroughly completed by introducing some reduction agents such as $NaBH_4$ (0.05 M in deionized water). As indicated in the TEM image (Figure 1D), a large amount of silver nanostructures was found on the titanate nanosubstrates. The color of the Ag/titanate nanocomposite at this stage has changed to black, which contributes mainly to a mass of polydispersed silver nanoparticles on the substrates (Figure 1H). Consistent with the electron microscopy image and mechanism analyses, the deconvolution of Ag $3d_{5/2}$ peak indicates that 45.91% of the original silver cations have been reduced to $Ag^{(0)}$, which has a typical binding energy at 368.2 eV, as depicted in Figure 3C. Accordingly, spectrophotometric measurements were also performed in order to follow the ion exchange and the reduction of Ag^+. Figure 4 shows the absorbance spectra of the various titanate-based compounds, which matches well with the observations shown in Figure 1.

Antimicrobial, antifungal, and antiproliferative activities

Studies examining bacterial inhibition zones in the presence of the titanate-based compounds were performed. The results for Ag/titanate in the presence of $NaBH_4$ reduction (A), Ag/titanate in the presence of UV light irradiation (B), and $Ag_2Ti_5O11 \cdot xH_2O$ (C), and pure $H_2Ti_5O_{11} \cdot H_2O$ (D) tested against E. coli, are presented as images in Figure 5. The Ag/titanate in the presence of UV light irradiation and $Ag_2Ti_5O_{11} \cdot xH_2O$ showed the highest antibacterial activity. The samples irradiated by the UV light have enhanced effects compared with the samples without UV
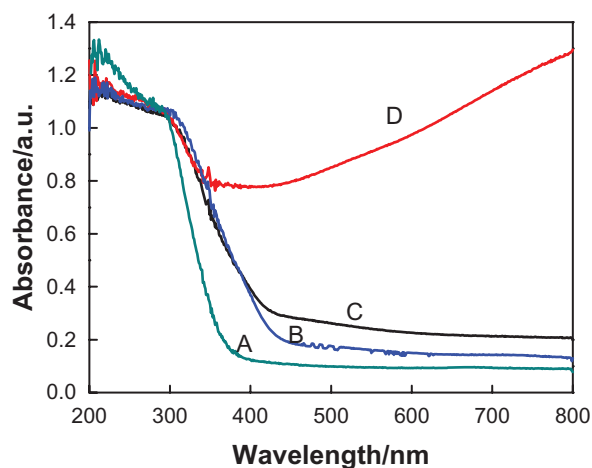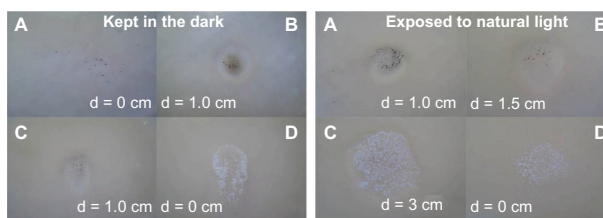

Figure 5 Comparison of the inhibition zone test for the titanate-based compounds: Ag/titanate by $NaBH_4$ reduction (**A**), Ag/titanate by UV light irradiation (**B**), $Ag_2Ti_5O_{11} \cdot xH_2O$ (**C**), and pure $H_2Ti_5O_{11} \cdot H_2O$ (**D**).

light irradiation. The fully protonated titanate ($H_2Ti_5O_{11} \cdot H_2O$) nanofibers showed the least effective antibacterial activity.

The results in Figure 6A show that both $Ag_2Ti_5O_{11} \cdot xH_2O$ and Ag/titanate (UV light irradiation) have excellent antifungal activity, as is revealed by the MIC_{50} values. For all titanate compounds containing silver, UV light irradiation can significantly enhance the antifungal activity. The MIC_{50} values of the samples irradiated by UV light are at least two-fold lower than those of the samples without UV light irradiation. The less than ideal antifungal activity of Ag/titanate ($NaBH_4$ reduction) might be due to the existence of fewer silver ions between the layers of the titanate nanofibers and the relatively large size of the silver nanoparticles decorating
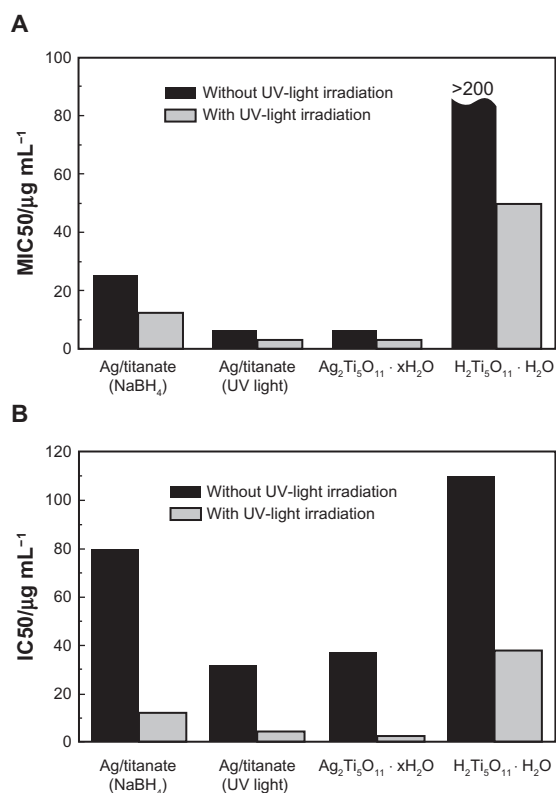

Figure 4 UV-visible absorption spectra of (**A**) protonated pentatitanate ($H_2Ti_5O_{11} \cdot H_2O$), (**B**) titanate after Ag^+ cations exchange, (**C**) partial reduction of Ag^+ cations from the layered space with the UV light irradiation, and (**D**) reduction of Ag^+ cations with $NaBH_4$ agent.

Figure 6 Antifungal (**A**) and antiproliferative (**B**) activities of titanate-based compounds, which are Ag/titanate by $NaBH_4$ reduction, Ag/titanate by UV light irradiation, $Ag_2Ti_5O_{11} \cdot xH_2O$, and pure $H_2Ti_5O_{11} \cdot H_2O$.

the surface. As a control sample, the fully protonated titanate ($H_2Ti_5O_{11} \cdot H_2O$) nanofibers show the worst antifungal activity, as expected, due to its low photocatalytic property and the absence of the silver ions. It should be noted that even though the FLC drug has the lowest MIC_{50} values (0.25 μg/mL respectively) in the presence of UV light irradiation, it is a small organic molecule and has undesirable effects including induction of drug resistance and instability. In view of this, the titanate nanofibers containing silver developed through the process reported here are still highly attractive and have no associated antimicrobial resistance issues as they are in a purely inorganic phase and have a totally different mechanism underpinning their antifungal activity.

Silver ions can readily deactivate bacteria by reacting with the thiol functional groups in proteases, which causes loss of integrity of the membrane, and then leads to malfunction of the permeability barrier.[5] This ultimately leads to the collapse of the bacterial membrane and the death of microorganisms. Furthermore, just like traditional photosensitizers, which have been widely applied in photodynamic therapy, titanate containing silver can also release highly reactive ROS to incapacitate the bacteria as well. For titanate nanofibers containing silver, the prolonged time of UV light irradiation may cause the formation of more silver nanoparticles on the surface of titanate nanofibers. However, this effect has been shown to be insignificant due to the relatively slow reduction process induced by UV light, which usually takes more than 10 hours. More interestingly, the as-prepared titanate nanocomposites containing silver also demonstrated good antiproliferative activities when tested in the human liver cancer cell line Hep G2 as a model target. As indicated in Figure 6B, both $Ag_2Ti_5O_{11} \cdot xH_2O$ and Ag/titanate (UV light irradiation) have better antiproliferative effects than those observed with Ag/titanate ($NaBH_4$ reduction) and plain titanate nanofibers, with the IC_{50} values being 32.28 and 37.51 μg/mL, respectively, without UV light irradiation. Moreover, the IC_{50} values can be further lowered to 4.79 and 2.53 μg/mL due to ROS-mediated cell damage; this is consistent with the antifungal activities discussed above. These promising antiproliferative activities of the inorganic titanates containing silver are also comparable to those found with purely organic drugs such as mitomycin C (MMC, $C_{15}H_{18}N_4O_5$); the IC_{50} values were 10.16 μg/mL (with UV light irradiation) and 12.21 μg/mL (without UV light irradiation), respectively.

The titanates containing silver developed in the process reported here appear to be quite unique, with the layered titanates having at least three functions: (i) acting as a reservoir for silver ions, which can be released continuously through the ion-exchange process; (ii) stabilizing the silver nanoparticles through the formation of silver-titanate nanocomposites; and (iii) generating ROS through the photocatalytic process, which can not only effectively enhance the antibacterial, antifungal, and antiproliferative activities, but also provide an environmentally friendly approach to in situ production of silver nanoparticles and avoid the oxidation of the silver species.

Conclusion

In conclusion, a series of titanate nanostructures containing silver with tailored compositions was successfully prepared through the ion-exchange method and controlled topochemical processes described, while their antibacterial, antifungal, and antiproliferative activities have been investigated in vitro. From the results, both $Ag_2Ti_5O_{11} \cdot xH_2O$ and Ag/titanate (UV light irradiation) have demonstrated excellent antibacterial, antifungal, and antiproliferative functional activities due to their unique structures and compositions, which include having photocatalytic activity to generate ROS and the ability to release silver ions continuously.

The soft chemistry strategy adopted in this working process may pave the way for the development of highly efficient, low-cost, and stable antimicrobial and antiproliferative agents with promise in applications such as producing a membrane for the treatment of superficial malignant tumors, esophageal cancer, or cervical carcinoma, and so on. They may also hold utility if incorporated into a coat on stents in moderate and advanced stage esophageal carcinoma or stents for endoscopic retrograde biliary drainage. These approaches may significantly reduce infections, inhibit tumor growth and, importantly, improve quality of life, and prolong survival time for patients with tumors.

Acknowledgments

Disclosure

The authors have no conflicts of interest to disclose in this work.

References

1. Chambers CW, Proctor CM, Kabler PW. Bactericidal effect of low concentrations of silver. *J Am Water Works Assoc*. 1962;54:208–216.
2. Russell AD, Huguo WB. Antimicrobial activity and action of silver. *Prog Med Chem*. 1994;31:351–370.

3. Applerot G, Lipovsky A, Dror R, et al. Enhanced antibacterial activity of nanocrystalline ZnO due to increased ROS-mediated cell injury. *Adv Funct Mater*. 2009;19:842–852.

4. Kittler S, Greulich C, Diendorf J, Köller M, Epple M. Toxicity of silver nanoparticles increases during storage because of slow dissolution under release of silver ions. *Chem Mater*. 2010;22:4548–4554.

5. Crespo-Monteiro N, Destouches N, Bois L, Chassagneux F, Reynaud S, Fournel T. Reversible and irreversible laser microinscription on silver-containing mesoporous titania films. *Adv Mater*. 2010;22:3166–3170.

6. Bragg PD, Rainnie DJ. The effect of silver ions on the respiratory chain of Escherichia coli. *Can J Microbiol*. 1974;20:883–889.

7. Banerjee M, Mallick S, Paul A, Chattopadhyay A, Ghosh SS. Heightened reactive oxygen species generation in the antimicrobial activity of a three component iodinated chitosan-silver nanoparticle composite. *Langmuir*. 2010;26:5901–5908.

8. Mao JY, Belcher AM, VanVliet KJ. Genetically engineered phage fibers and coatings for antibacterial applications. *Adv Funct Mater*. 2010;20:209–214.

9. Shang L, Li BJ, Dong WJ, et al. Heteronanostructure of Ag particle on titanate nanowire membrane with enhanced photocatalytic properties and bactericidal activities. *J Hazard Mater*. 2010;178:1109–1114.

10. McDonnell G, Russell AD. Antiseptics and disinfectants: activity, action, and resistance. *Clin Microbiol Rev*. 1999;12:147–179.

11. Grippaudo FR, Carini L, Baldini R. Procutase versus 1% silver sulph-adiazine in the treatment of minor burns. *Burns*. 2010;36:871–875.

12. Liong M, France B, Bradley KA, Zink JI. Antimicrobial activity of silver nanocrystals encapsulated in mesoporous silica nanoparticles. *Adv Mater*. 2009;21:1684–1689.

13. Pang ML, Hu JY, Zeng HC. Synthesis, morphological control, and antibacterial properties of hollow/solid Ag_2S/Ag heterodimers. *J Am Chem Soc*. 2010;132:10771–10785.

14. Lv M, Su S, He Y, et al. Long-term antimicrobial effect of silicon nanowires decorated with silver nanoparticles. *Adv Mater*. 2010;22: 5473–5467.

15. Sasaki T, Komatsu Y, Fujiki Y. Protonated pentatitanate: preparation, characterizations, and cation intercalation. *Chem Mater*. 1992;4:894–899.

16. Bavykin DV, Friedrich JM, Walsh FC. Protonated titanates and TiO_2 nanostructured materials: synthesis, properties, and applications. *Adv Mater*. 2006;18:807–2824.

17. Cesano F, Bertarione S, Uddin MJ, Agostini G, Scarano D, Zecchina A. Designing TiO_2 based nanostructures by control of surface morphology of pure and silver loaded titanate nanotubes. *J Phys Chem C*. 2010;114: 169–178.

18. Li QY, Kako T, Ye JH. Strong adsorption and effective photocatalytic activities of one-dimensional nano-structured silver titanates. *Appl Cata A*: *Gen*. 2010;375:85–91.

19. Sasaki T, Watanabe M, Komatsu Y, Fujiki Y. Layered hydrous titanium dioxide: potassium ion exchange and structural characterization. *Inorg Chem*. 1985;24:2265–2271.

20. Sun XM, Li YD. Synthesis and characterization of ion-exchangeable titanate nanotubes. *Chem Eur J*. 2003;9:2229–2238.

21. Morgado EJ, Abreu MAS, Moure GT, Marinkovic BA, Jardim PM, Araujo AS. Characterization of nanostructured titanates obtained by alkali treatment of TiO_2-anatases with distinct crystal sizes. *Chem Mater*. 2007;19:665–676.

22. Bavykin DV, Walsh FC. Kinetics of Alkali metal ion exchange into nanotubular and nanofibrous titanates. *J Phys Chem C*. 2007;111: 14644–14651.

23. Inoue Y, Uota M, Torikai T, et al. Antibacterial properties of nano-structured silver titanate thin films formed on a titanium plate. *J Biomed Mater Res A*. 2010;92A:1171–1180.

24. Ma RZ, Sasaki T, BandoY. Layer-by-Layer assembled multilayer films of titanate nanotubes, Ag- or Au-loaded nanotubes, and nanotubes/nanosheets with polycations. *J Am Chem Soc*. 2004;126:10382–10388.

25. Su YH, Qiao SZ, Yang HG, et al. Titanate–silica mesostructured nanocables: synthesis, structural analysis and biomedical applications. *Nanotechnology*. 2010;21:065604.

26. Wang QG, Gao QM, Shi JL. Enhanced catalytic activity of hemoglobin in organic solvents by layered titanate immobilization. *J Am Chem Soc*. 2004;126:14346–14347.

27. Dai H, Chi YW, Wu XP, Wang YM, Wei MD, Chen GN. Biocompatible electrochemiluminescent biosensor for choline based on enzyme/titanate/chitosan composite modified electrode. *Biosens Bioelectron*. 2010;25:1414–1419.

28. Dong WJ, Zhang TR, Epstein J, et al. Multifunctional nanowire bioscaf-folds on titanium. *Chem Mater*. 2007;19:4454–4459.

29. Wataha JC, Hobbs DT, Lockwood PE, et al. Peroxotitanates for biode-livery of metals. *J Biomed Mater Res B*. 2009;91:489–496.

30. Yang HG, Zeng HC. Synthetic architectures of TiO_2/$H_2Ti_5O_{11} \cdot H_2O$, ZnO/$H_2Ti_5O_{11} \cdot H_2O$, ZnO/TiO_2/$H_2Ti_5O_{11} \cdot H_2O$ and ZnO/TiO_2 nanocomposites. *J Am Chem Soc*. 2005;127:270–278.

31. Nakamura K, Niimi M, Niimi K, et al. Functional expression of *Candida albicans* drug efflux pump Cdr1p in a *Saccharomyces cerevisiae* strain deficient in membrane transporters. *Antimicrob Agents Chemother*. 2001;45:3366–3374.

32. Gu W, Han KQ, Su YH, Huang XQ, Ling CQ. Inhibition action of bufalin on human transplanted hepatocellular tumor and its effects on expressions of Bcl-2 and Bax proteins in nude mice. *J Chin Integr Med*. 2007;5:155–159.

33. Ling CQ, Su YH. Possibility and necessity of constructing new nano-formula systems of traditional Chinese medicine. *J Chin Integr Med*. 2010;8:101–105.